Journal of Research of the National Bureau of Standards Vol. 55, No. 3, September 1955 Research Paper 2615

Atomic Negative-Ion-Photodetachment Cross-Section and Affinity Measurements [1]

Stephen J. Smith and Lewis M. Branscomb

The spectral distributions of the H^- and O^- cross sections for photodetachment have been measured. The H^- measurements are consistent with the theory of Chandrasekhar. A curve has been fitted to the results for O^-. The threshold of this cross section, the affinity of O^-, is found to be 1.48 ± 0.10 electron volts. No evidence is found for resonance at the threshold or for the existence of excited O^- ions. The apparatus is described in detail.

1. Introduction

The observation in this laboratory of the photodetachment of electrons from negative ions in 1953 [1] [2] opened the possibility of studying the absorption spectra of negative ions. The first application of the technique was to the determination of the absolute absorption by H^-, integrated over a wide spectral range [2]. The results agreed with the theoretical predictions of Chandrasekhar and his colleagues [3]. In our H^- experiments the principal task was accurate calibration of the equipment for the absolute measurement of the integrated cross section.

This paper discusses measurements of the spectral distributions of photodetachment cross sections. These are of interest not only because of their practical applications to astrophysics and geophysics, but also because of the information that can be obtained about the electron affinities of atoms and the possible existence of excited states of negative ions. For unexcited atomic negative ions the wavelength of the threshold for photodetachment corresponds to the electron affinity of the atom. The shape of the photodetachment cross section near the threshold supplies information about the possibility of excited states of the negative ion [4, 5]. From this curve one can also determine the radiative attachment cross section from the principle of detailed balancing [6]. This is of particular interest for studies of ionospheric electron density.

A preliminary value for the oxygen affinity has been obtained [7] by this method. This paper describes the details of the procedure for determining the affinity and the shape of the detachment cross-section curve, and summarize the spectral-distribution measurements for H^- and O^-. Because the method does not uniquely determine the wavelength dependence of the cross section, sufficient data is given to permit the reader to test the compatibility of any proposed cross section and our experimental data. The first H^- paper [2] gives details of the method of calibrating the apparatus for measuring absolute cross sections.

The experimental techniques peculiar to these measurements, as contrasted with experiments on neutral atoms or positive ions, stem from two characteristics of *atomic* negative ions: (1) the low binding energies; and (2) the finite number, usually only one, of bound states. These characteristics are attributed to the weak short-range forces responsible for the stability of negative ions [8].

Because of the low binding energies it is difficult to produce useful quantities of negative ions. The atomic processes for producing them must generally compete with more probable reactions, and such ions as are produced are easily destroyed.

The practical result of the limited number of bound states is that transitions in most atomic negative ions are confined to those between the ground state and the continuum. For those negative ions that have only one bound state, for example, the negative atomic hydrogen ion, all excitations result in the complete detachment of the excess electron. In principle, these ions might be studied equivalently from the points of view of absorption spectroscopy or of ion destruction. The threshold for absorption of photons is the same as the affinity, and the study of the intensity distribution of the absorption spectrum is equivalent to a study of the energy spectrum of the detached electrons.

A few atomic negative ions may have more than one bound state. There is some experimental evidence that negative atomic oxygen is one of these [9, 10, 11]. In such a case a study of the photon absorption spectrum, if it were feasible, would give more complete information than would the photodetachment spectrum.

In practice, negative ions can be produced only in such small quantities ($\sim 10^{-7}$ amp) that the fraction of incident photons actually absorbed in a realizable experiment is difficult to observe directly; particularly as the spectrum is continuous. Negative-ion photoexcitation, therefore, is naturally studied from the point of view of ion destruction, either by observation of the neutral atoms created in an illuminated negative-ion beam or by observation of the detached electrons.

In the experiment described in this paper, the detached electrons are observed. The apparatus was designed for measurements of an absolute cross section, requiring the collection of all detached elec-

[1] Supported in part by the Office of Naval Research.
[2] Figures in brackets indicate the literature references at the end of this paper.

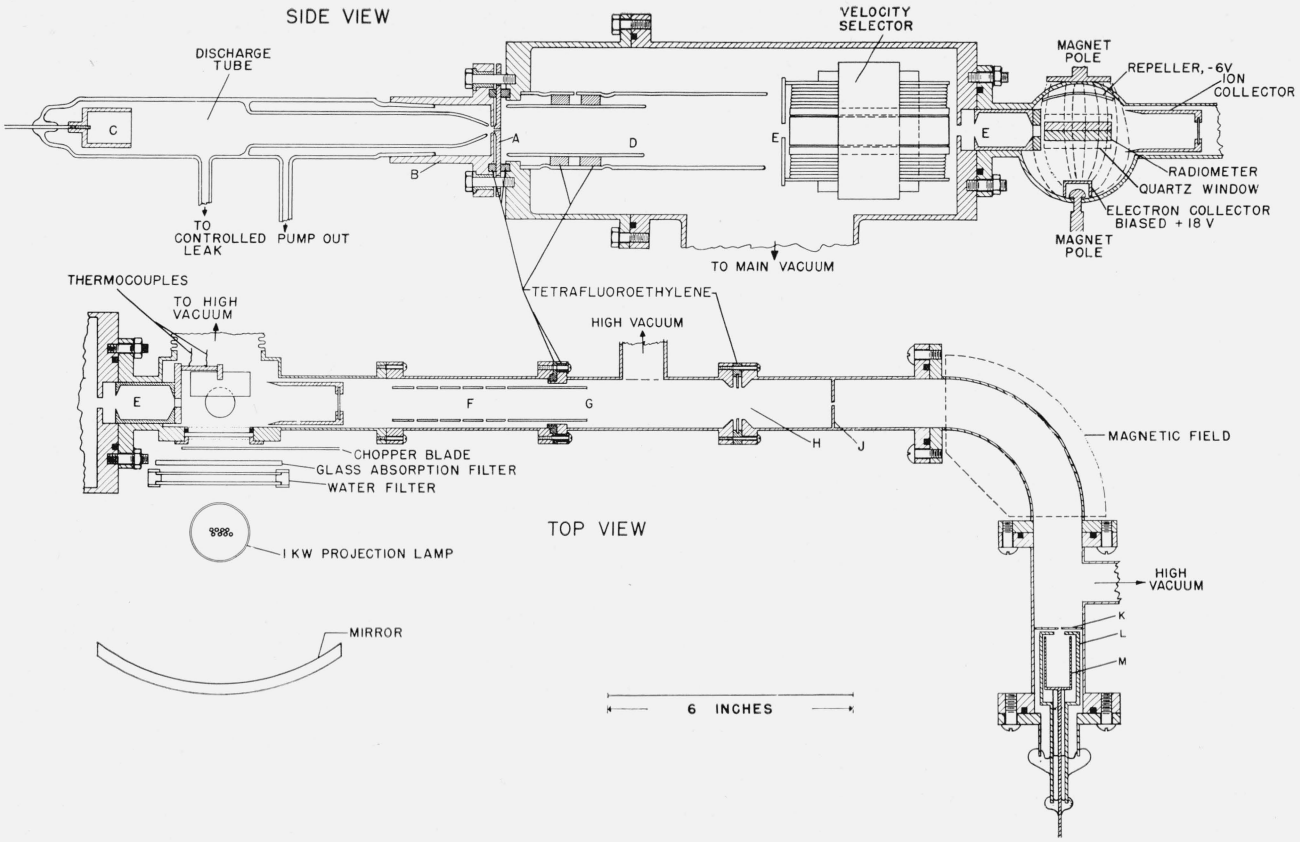

FIGURE 1. *Schematic drawing of the apparatus showing elements of the ion and photon beam optics.*

The ion beam is produced in the gas discharge tube (pressure $\leq$100 Hg) by applying up to 6 kv between A, the anode, and C, the cathode. A is biased 100–200 v negative with respect to ground potential. C, the control electrode, is biased as much as 500 v negative with respect to A. D, operated about 2,500 v positive, forms an electrostatic lens with the surrounding elements; focusing the ion beam through defining apertures, E.

The ions not deflected by the velocity selector (see also fig. 4) pass through the reaction chamber into the ion collector. The back of the ion collector may be opened to allow the beam to pass into a 90° sector-field mass spectrometer. F, G, and H are an ion optical system designed to render the beam parallel at the entrance slit J, independent of mass. Lens F gradually accelerates the ions to a fixed fraction of their final energy. Lens G accelerates the ions to the proper energy to obtain a focus at the exit slit K of the mass spectrometer. The vacuum housing forms part of the lens G and that part beyond G is at high voltage. Unipotential lens H compensates for the focusing power of G. Those ions focussed on K by the magnetic field are collected in M, at ground potential. L, which shields M, is biased −67 v.

Two interchangeable magnets are used with the spectrometer. One, with a field of 3,300 gauss, is used for heavy ions; and the other, with a field of 1,100 gauss, is used for light ions. Tetrafluoroethylene resin is used where vacuum gaskets must also serve as electrical insulators. These gaskets are used where indicated and also to insulate electrically the mass spectrometer housing beyond G from the grounded high vacuum pumps and traps.

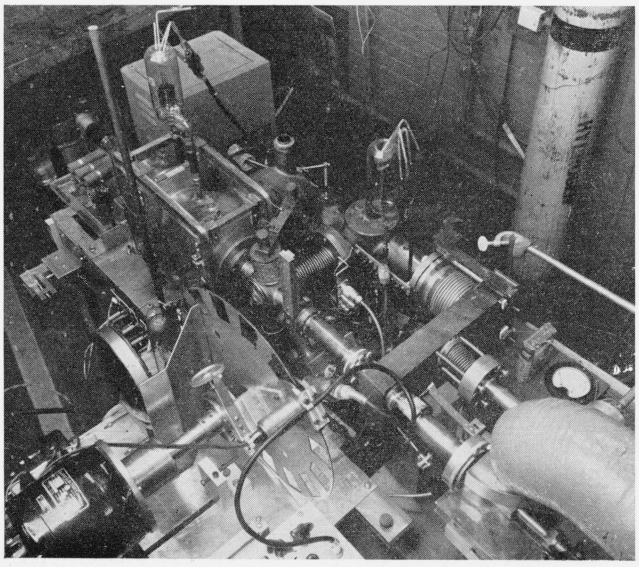

trons. For simplicity the observation of the energy spectrum of the detached electrons is not attempted, but the spectrum is deduced from the dependence of the total detached electron current on the spectral distribution of the incident photons.

The apparatus, particularly its application to integrated absolute cross sections, has been described [2]. Those features of the apparatus of particular importance for the determination of affinities and spectral distributions of cross sections are dealt with here in greater detail.

The apparatus is shown schematically in figure 1 and photographically in figure 2. A mass-separated ion beam crosses a very intense photon beam. The photon beam is chopped, and the current of detached electrons is measured with a frequency- and phase-discriminating amplifier, in order to separate the

FIGURE 2. *Over-all view of the apparatus.*

The chopper-lamp-mirror assembly is shown pulled back about 6 in. from its operating position.

photodetachment current from background currents. The average value of the chopped detachment current is compared with the direct ion current. A mass spectrometer built into the apparatus provides for analysis of the ion beam.

Monochromatic sources of radiation of adequate intensity have not been available. Therefore the radiation continuum from a hot wolfram filament is used, and changes in spectral distribution are accomplished with sharp-cutoff filters. A radiometer [2] measures the total radiant power incident on the beam.

2. Operation of the Experiment

2.1. Photon Beam

The light source is a 1–kw projection lamp [2] operating at a measured [3] color temperature of 3,420° K, corresponding to an absolute temperature of 3,300° K [12, 13]. The spectral-intensity distribution of this source was obtained by multiplying the 3,300° K Planck curve by the measured [4] transmission of the quartz envelope and by the best available values of the emissivity of the wolfram filament material, from 3000 A to 40000 A at 3,300° K [14].

Radiation from the lamp is focused by a front-aluminized spherical mirror, through a quartz window, into the negative-ion beam. A low-sensitivity platinum-blacked radiometer, located behind the ion beam measures the radiant power in the photon beam. The radiant power at the ion beam is about 30 w when no optical filtering is used.

The spectral distribution of the photon beam emitted by the projection lamp can be altered by means of optical filters. A set of polished Corning glass absorption filters and one Baird infrared multilayer reflection filter with measured transmissions [3] are used in this work. The transmissions of these filters and the spectral distribution of the lamp are illustrated in figure 3.

When the H^- cross section was measured, the water filter shown in figure 1 was not available. It is clear from figure 3 that the filters were required to absorb a large fraction of the 100 to 200 w of radiation incident on them. This resulted in severe local heating—especially in the infrared filters, which invariably broke under prolonged use with only air cooling. It is known also that the transmissions of the glass absorption filters, and their cutoff wavelengths, are temperature dependent [15]. Spectroscopic examination of transmitted light shows that the cutoff wavelengths shift toward the infrared when the filters are placed in the full photon beam. In the infrared-absorption filters the shift is about 120 A, and in the yellow filters it is of the order of 50 A.

For the O^- measurements the water filter was inserted in the photon beam in front of the filters. This reduced transmission shifts and allowed full use of the filters by absorbing the infrared beyond about 1.25 μ. Distilled water, kept at constant temperature by a heat exchanger, is circulated through the 6-mm-deep space between the two polished glass faces of the water cell. As an extra precaution the measurements with each infrared filter were made by using that filter as the back face of the water cell in place of a clear glass plate. The transmission of the water cell (see footnote 3) was found to be nearly constant (86 to 90%) and independent of moderate temperature changes over the spectral range in which O^- photodetachment occurs

[3] Measured by the NBS Photometry and Colorimetry Section.
[4] Measured by the NBS Radiometry Section.

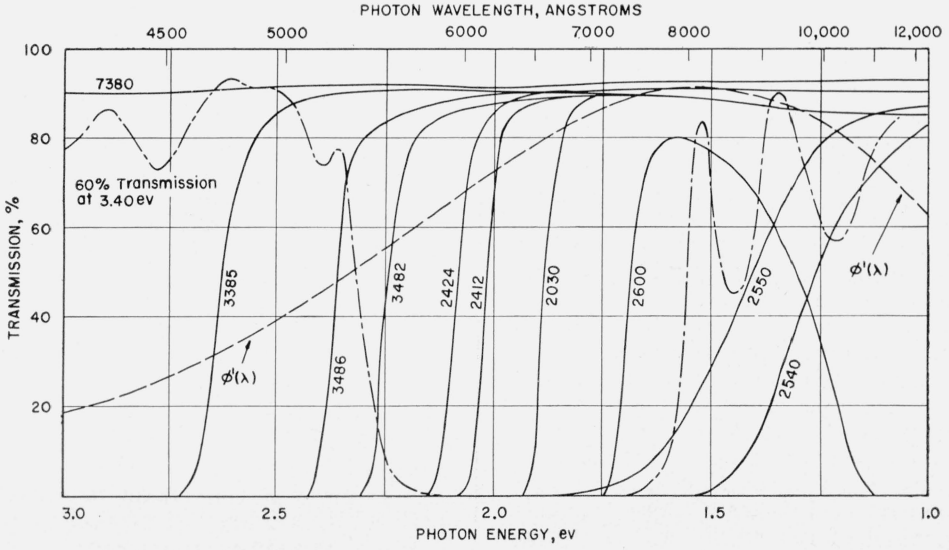

FIGURE 3. *Filter transmissions.*

The solid lines show the transmissions of the Corning glass absorption filters. The dot-dash line is the transmission of the Baird interference reflection filter. The dashed line gives the spectral distribution $\phi'(\lambda)$ of the radiation from the projection lamp.

2.2. Electron-Current Collection

Electrons are detached from the ions at the intersection of the ion and photon beams. A 50-gauss magnetic field in the region of intersection traps the detached electrons. These have very low energy because of the small excess of $h\nu$ over the detachment threshold energy (the affinity). (The velocity along the ion beam is negligible.) Ions of 200-v energy are deflected with a minimum radius of curvature approximately equal to 50 cm/amu, and are deflected only 1 or 2 mm at the ion collector.

The magnetic-field lines from all points of the region of the beam intersection converge onto a small electrode, where the electron current is collected for measurement (see fig. 1). This collector is biased +18 v, and a repeller plate on the opposite side of the beam is biased −6 v.

The electron collector may receive currents that are derived from the ion beam by several processes other than photodetachment: (a) collisional detachment of electrons from negative ions, (b) production of charge-exchange ions with low energy, (c) ion scattering by the residual gas in the chamber, and (d) production of secondary electrons from scattered ions. Although unmodulated by the light chopper, these undesired currents may produce large noise signals.

Collisional detachment produces low-energy electrons in the region of intersection of the beams. These will all be collected, as will charge-exchange ions in this region. Scattered ions, having higher energy, will not be trapped in the weak inhomogeneous magnetic field and should not be important, because the collector subtends a small solid angle in a direction perpendicular to the direction of the beam. Secondary electron current reaching the collector is probably considerably smaller than total scattered ion current.

The cross sections for some of these negative-ion processes have been measured in a few special cases, and these results are not directly applicable here. For an order-of-magnitude estimate of the background current to the electron collector, we use a typical collisional detachment cross section of 20 cm^{-1} (at 1-mm pressure) [10]. At normal operating pressure of 10^{-6} mm Hg and with an ion-beam current of 10^{-7} amp, the estimated background current collected from 5 cm of ion-beam path is about 10^{-11} amp. The magnitude of the photodetachment current is approximately 10^{-12} amp.

In these measurements the photodetachment current is separated from other ion-beam-dependent effects by chopping the photon beam at 450 cps and observing the photodetachment current with a frequency- and phase-discriminating narrow-band amplifier. This coherent photodetachment signal is observed against a background of noise derived from the component of ion-beam noise that lies within the pass band of the amplifier. If the ion-beam noise is a thousand times shot noise [16], the background-noise current is approximately

$$I^2 = 2\times10^3\, e\, I\Delta f,$$

where e is the electronic charge of 1.6×10^{-19} coulomb, I is the current in amperes, and Δf is the amplifier bandwidth. For a 10^{-1}-cps bandwidth the noise current would be about 10^{-14} amp, or about one hundredth of the typical observed photodetachment signal. A typical observed signal-to-noise ratio is 50 to 1.

Photoelectric effect at metal surfaces can produce a coherent 450-cps current to the electron collector. With no filters in the photon beam, the chopped photoelectric current may be several times larger than the photodetachment current. The insertion of any of the filters reduces the photoelectric effect to the magnitude of the photodetachment signal or smaller. Furthermore, with the filters, the small photoelectric current is by chance approximately 90° out of phase with the photodetachment signal. This is presumably because the rotating chopper allows the photon beam to reach a low work-function surface at the top of the reaction chamber before it reaches the ion beam. Most surfaces are nickel plated and have photoelectric thresholds beyond the cutoff wavelengths of the filters. In practice, the in-phase component of the photoelectric current is at most only a few percent of the photodetachment signal. It is easily measured by turning off the ion beam and observing the effect of the photon beam alone.

Photodetachment of those ions created by charge exchange in the reaction chamber should not produce a coherent 450-cps signal, because all charge-exchange ions or their photodetached electrons are collected. This is demonstrated by the saturation of the 450-cps current to the electron collector with an increase from zero of the electric and magnetic fields in the reaction chamber. In addition the concentration of such ions must be extremely small.

Scattered ions and other stray charges striking the inside of the quartz window would cause fluctuating potentials to build up on the glass surface, disturbing the electrostatic field used to collect the photodetached electrons. For this reason, and to eliminate capacitive pickup between the electron collector and the blades of the chopper, a fine knitted mesh of 0.001-in. wolfram wire was stretched over the quartz window.

2.3. Ion Beam

The ions are produced in the positive column of a low-pressure glow discharge. The discharge tube is an adaptation of one described by Fite [16]. A steady voltage of 2 to 8 kv is applied across the discharge. The control electrode, designed to concentrate negative ions on the axis of the tube, is biased negative with respect to the anode. The ions that pass through the anode channel to form the beam, originate at a potential about 100 v negative with respect to the anode potential. The anode potential is variable with respect to ground to afford control of the ion-beam energy.

An electrostatic lens, coaxial with the beam, accelerates the ions to about 2 kv and then decelerates them into a region of ground potential. This lens

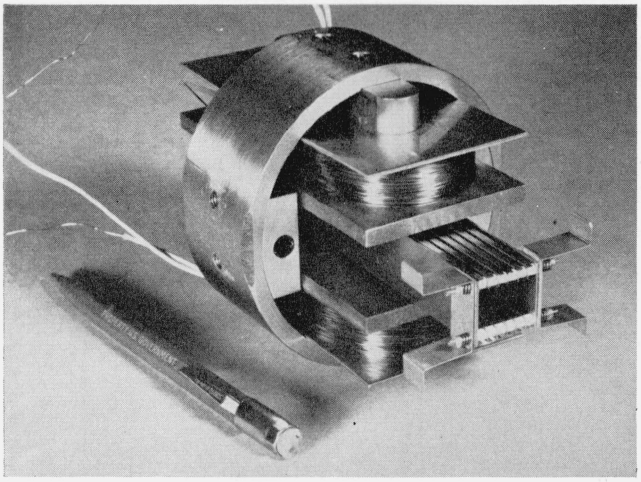

FIGURE 4. *Crossed field velocity selector used for mass separation of ions.*

The *E*-field electrodes are pulled out from the magnet pole faces to show details of the guard strips which maintain a homogeneous electric field. The potentials are distributed on these guard strips by a voltage divider made of 3,000 ohm Corning glass resistors in the vacuum.

renders the beam parallel or slightly convergent.

After being focused, the beam passes along the axis of the crossed-field velocity selector shown in figure 4. In this region weak magnetic fields can be applied from coils external to the vacuum to correct the alinement of the beam.

At the end of the velocity selector, three apertures remove the peripheral and highly divergent rays from the beam, which then passes into the detachment chamber, crosses the photon beam, and is caught in a Faraday cup. A weak transverse magnetic field and a small positive bias on the Faraday cup trap the secondary emission, so that the beam current (ordinarily from 25 mμa to nearly 1 μa) can be accurately measured. The magnitude and spread of the ion energy are determined by measuring the beam current while applying repelling potentials to the cup.

A shutter in the Faraday cup can be opened magnetically to allow part of the beam to pass into a 90°-sector-field mass spectrometer. This instrument is of conventional design, and its elements are shown in figure 1.

2.4. Ion-Beam Purity

The purity of the beam was controlled in two ways. A low-dispersion mass separator (the crossed-field velocity selector) was built into the apparatus; and for the O^- measurements spectroscopically pure gas was used in the discharge tube. In addition, the purity of the beam was subjected to repeated experimental checks.

The mass separator, shown in figure 4, is a crossed-field instrument in which a uniform electric field ($\leq$60 v/cm) opposes the deflecting force of the uniform magnetic field ($\leq$500 gauss). These fields are adjustable to allow ions having a chosen velocity to pass through undeflected. The mass-separating action depends on the experimental observation that ions of different species have approximately equal energies (see fig. 5); thus each ion has a characteristic velocity. The dispersion of this instrument depends on the length of ion path in the crossed fields and on the strength of the fields.

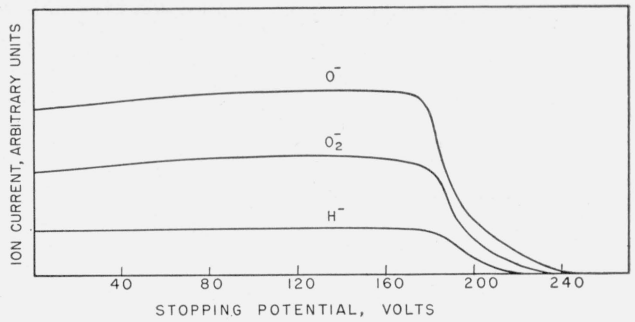

FIGURE 5. *Ion current versus stopping potential at the ion collector for several ion species from the same discharge.*

This example shows an energy spread greater than that usually obtained. All ion species appear to originate at the same potential in the plasma.

a. H^--Beam Purity

The H^- measurements were made with wet tank hydrogen or with D_2O in the discharge tube. With a 500-gauss magnetic field the velocity-selector dispersion was great enough for the separation of H^- from D^-, and D^- from O^- and heavier ions that also came from the discharge tube (fig. 6). This purity was studied by scanning the mass spectrum with the analyzing spectrometer while the velocity selector was peaked on H^- or D^-. Any impurities present were less than 0.1 percent of the ion beam.

Because ion impurities could strike the ion collector on one edge even though deflected sufficiently by the velocity selector to miss the entrance to the mass spectrometer, further verification of beam purity was necessary. The ratio of photodetachment current to ion current was independent of the dispersion of the velocity selector. Furthermore, the ratio of the photodetachment current to ion current was constant over the useful part of the H^- peak (fig. 6) obtained with the velocity selector.

b. O^--Beam Purity

Photodetachment from oxygen ions was studied in detail by using ions drawn from an oxygen discharge. After this work was completed, the oxygen affinity was redetermined, using ions from a carbon-monoxide discharge. These results are described in section 5.

For the O^- experiments, using an oxygen discharge, the velocity selector dispersion was great enough to separate O^- from O_2^-, and from H^- and D^-. However, the analyzing spectrometer showed masses 17 and 18 still present when the velocity selector was selecting O^- with largest available dispersion.

To achieve the required purity of the beam it was necessary to outgas the gas-handling system and the discharge tube carefully, and to use spectroscopically pure gas in the discharge.

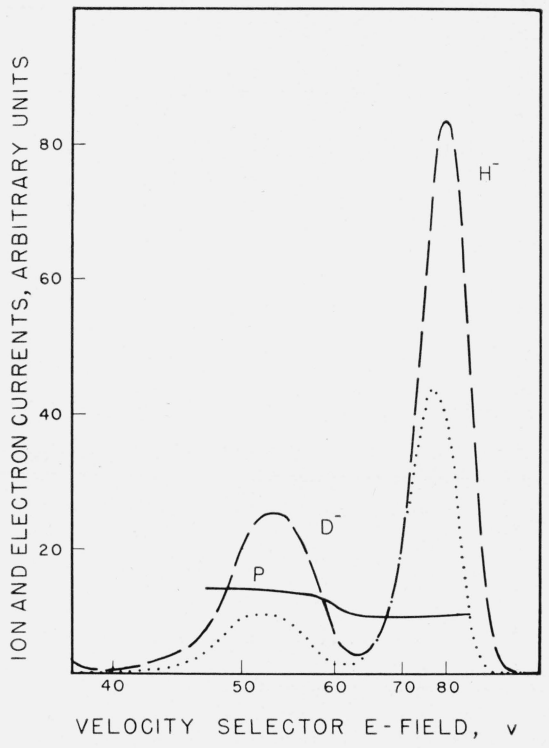

FIGURE 6. *Velocity selector scan of the ion beam from an* H_2, D_2O *discharge.*

The dashed line shows the current to the ion collector as the electrostatic *E*-field is varied, with constant magnetic field H=150 gauss. The horizontal scale shows the number of volts across the 1.9-cm gap between the deflector plates. The scan was run with the photon beam turned on, and the dotted line shows the photodetachment current (slightly displaced by the recording mechanism and enlarged relative to the ion current by about 10^5). The solid line is the measured ratio, P, of detachment current to ion current on an arbitrary scale. P is approximately constant over each peak, and $P_{D^-}/P_{H^-}=v_{H^-}/v_{D^-}=1.41$. Other careful measurements show P is accurately constant over each mass peak.

Because the gas-handling system could not be baked, outgassing was accomplished by about 20 hr of pumping, down to pressures as low as 5×10^{-6} mm Hg. The glass discharge tube was outgassed in the same way. The cathode was baked out with an induction heater. The anode and control electrode were outgassed by about 30 hr of operation of the discharge with the pure oxygen.

At the end of this time, with the velocity selector turned off, the analyzing spectrometer showed large O^-, O_2^-, and some heavier peaks. There were also traces of masses 17, 18, and 19 (fig. 7), presumably due to OH^-, OD^-, O_{18}^-, and F^-. The latter is probably from the electrically insulating tetrafluoroethylene gaskets used in the vacuum system. These trace peaks were of the order of 0.2 percent as high as the O^- and O_2^- peaks.

In the work on the O^- affinity it was particularly important to demonstrate that the O^- beam contained no O_2^-. The separation of O^- from O_2^- was checked by demonstrating that the ratio of detachment current to ion current is independent of the dispersion of the velocity selector over a reasonable range of dispersions, and constant over the useful part of the O^- mass peak (fig. 8). The O_2^- ion itself was studied. Its cross section and detachment

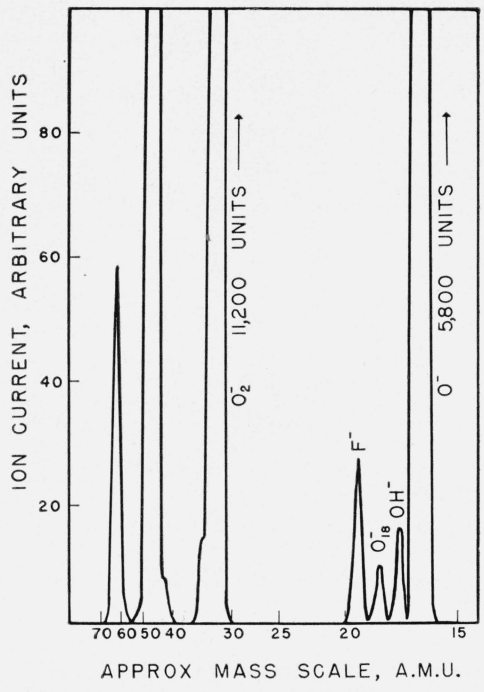

FIGURE 7. *Mass spectrum of the ion beam from an* O_2 *discharge.*

This spectrogram was taken with the 90° sector-field spectrometer. The resolution of the instrument is not high enough to allow exact determination of the mass numbers associated with the two heavy peaks. These could be NO_2^- and NO_3^- at masses 46 and 62 although no nitrogen was admitted to the spectroscopic oxygen, and nitrogen was not observable in the optical spectrum of the discharge. They could also be masses 48 and 64, although observation of O_3^- and O_4^- is not described in the literature, and the discharge pressure was less than 50 μ of Hg.

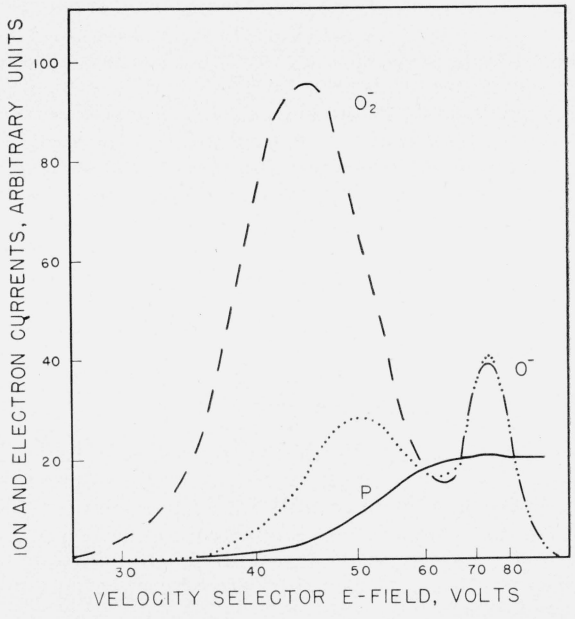

FIGURE 8. *Velocity selector scan of the ion beam from an* O_2 *discharge.*

The dashed line shows the current to the ion collector as the *E*-field is varied, with constant H=500 gauss. The high-field side of the large peak is O_3^-, and the low field side is composed of heavier ions (see fig. 7). The dotted line shows the corresponding photodetachment current (slightly displaced and magnified by about 10^5). The solid line is the measured ratio, P, of detachment current to ion current on an arbitrary scale. The constancy of P over the O^- peak has been verified by other measurements.

threshold were shown to be markedly different from those of O^-. The O_2^- cross section was somewhat lower and the detachment threshold lay farther into the infrared, beyond the limits of our infrared filter cutoffs.

3. Procedure for Data Analysis

The experimental probability that an ion, in passing through the photon beam, loses its extra electron is the ratio of the detached-electron current to the negative-ion current. This photodetachment probability is designated P_{exp}. It is a function of the specific geometry and conditions of the experiment.

A theoretical detachment probability, P_{theo}, that applies to our geometry has been derived [2]:

$$P_{theo}=0.317\times10^{13}W_0(M/E)^{1/2}\int\sigma(\lambda)\phi'(\lambda)T_n(\lambda)\lambda d\lambda. \quad (1)$$

Here W_0 is the power in watts of the unfiltered radiation falling on the radiometer; M is the mass of the negative ion in atomic mass units, and E is its mean energy in electron volts; $\phi'(\lambda)$ is the spectral distribution. in microns^{-1}, of the photon source, normalized to unity; T_n (λ) is the transmission of the n^{th} filter when placed in the light beam; and λ is the wavelength, in microns. The cross section, $\sigma(\lambda)$, is in square centimeters. To test the accuracy of a proposed cross section, $\sigma(\lambda)$, the prediction of eq (1) is compared with the experimental detachment probability. We followed this procedure in the H^- work, using the theory of Chandrasekhar.

If $\sigma(\lambda)$ has not been calculated but can be presumed to be a slowly varying function of λ, $\sigma(\lambda)$ can be determined from successive differences of P_{exp} in that region of the spectrum for which sharp-cutoff filters are available. These filters must have transmission curves that maintain their maximum values to wavelengths at least as long as the threshold wavelength corresponding to the affinity. If filters a and b have sharp-cutoff characteristics and identical maximum transmissions, the difference between the experimental detachment probabilities for these filters is predicted by the equation

$$P_a-P_b=\Delta(P_{exp})=$$

$$0.317\times10^{13}W_0(M/E)^{1/2}\int\sigma(\lambda)\phi'(\lambda)(T_a-T_b)\lambda d\lambda. \quad (2)$$

Here we have assumed that the radiation power, W_0, and ion energy, E, are each the same in the two measurements. If this is not true, we must write

$$\left(P_{exp}\frac{E^{1/2}}{W_0}\right)_a-\left(P_{exp}\frac{E^{1/2}}{W_0}\right)_b=$$

$$0.317\times10^{13}M^{1/2}\int\sigma(\lambda)\phi'(\lambda)(T_a-T_b)\lambda d\lambda. \quad (3)$$

The cross section is then

$$\sigma(\lambda)\doteq\frac{\Delta(P_{exp}E^{1/2}W_0^{-1})}{0.317\times10^{13}M^{1/2}\int\phi'(\lambda)\Delta[T(\lambda)]\lambda d\lambda}\ \text{cm}^2. \quad (4)$$

If the maximum transmissions of the filters are not equal, (4) is modified as follows:

$$\sigma(\lambda)\doteq\frac{\Delta(P_{exp}T_{max}^{-1}E^{1/2}W_0^{-1})}{0.317\times10^{13}M^{1/2}\int\phi'(\lambda)\Delta\left[\frac{T(\lambda)}{T_{max}}\right]\lambda d\lambda}\ \text{cm}^2. \quad (5)$$

The difference method of determining $\sigma(\lambda)$ is not applicable in the near infrared with our absorption filters (see fig. 3). Only the selenium-glass filters with cutoff wavelengths between 4500 and 7000 A have the required transmission characteristics. For negative ions with detachment thresholds less than 1.3 ev the difference method encounters additional serious difficulties. This occurs even in the determination of the cross section in the visible spectrum, because of the slight decrease in filter transmission and the marked increase in the water-cell absorption near 0.9μ. Combined with the rapid increase with rapid increase with wavelength of the product, $\lambda\phi'(\lambda)$, this causes the difference in P_{exp}'s of two filters to arise from two widely separated regions of the cross section, introducing ambiguity in every measurement.

The affinity usually given in the literature for O^- is about 2.2 ev [17]. For this reason we used the difference method in the visible spectrum. In the near infrared region of the O^- photodetachment cross section the procedure was to adopt a reasonable monotonic trial function, $\sigma'(\lambda)$, for integration of eq (1), and to make successive adjustments of the trial function for best fit with the experimental data.

The theoretical affinity for hydrogen is 0.747 ev [3], and the detachment threshold of O_2^- is smaller than 1.3 ev. For this reason the difference method was not applied to H^- or to O_2^-.

4. Experimental Results

4.1. Results for H^-

Two sets of measurements have been made of the spectral dependence of the H^- cross section for photodetachment, using the glass absorption filters. In the preliminary set the filters were taken in random order with all measurements on a given filter taken consecutively. In the second set the filters were taken in a scrambled order. The order was rescrambled after a cycle of one measurement per filter. Eleven complete cycles were carried through.

The results are not on an absolute basis. They are given relative to the value obtained for filter 3486. We have previously described absolute measurements of the integrated cross section for H^-, using filter 3486 and filter 2412 [2]. The theory

of Chandrasekhar is used to provide a test cross section in the integration of eq (1) for the comparison with the experimental results shown in table 1. The conclusion that the trend evident in the more recent data reflects an error in the shape of Chandrasekhar's H^- cross section is not justified because of uncertainty in $\phi'(\lambda)$ and in the temperature coefficients of the filters. The experimental results are in general agreement with the theory.

4.2. Results for O^-

We have made two sets of measurements of the spectral dependence of the O^- photodetachment cross section, using the glass absorption filters and ions from an oxygen discharge. In the first set the filters were cycled 13 times in order of increasing cutoff wavelengths. In the second set the filters were rescrambled for each of 8 cycles, the order being carefully chosen to minimize the effect of long and short time drifts in the differences between probabilities for filters with adjacent cutoff wavelengths.

These measurements were made on a relative basis. Subsequently, absolute measurements were made with filter 3486 by the method described [2]. The results of the relative measurements in table 2 are therefore given on an absolute basis. The measured absolute values of the cross sections are estimated to be reliable within ± 10 percent [2].

The two sets of results are combined in table 2 because the ratios of photon-beam power, W_0, to the ion velocity ($\sim E^{\frac{1}{2}}$) were the same (see eq (1)) in both sets of measurements. Table 3 gives the transmission and photon spectral-distribution data necessary for the integration of (1) with arbitrary trial cross sections for comparison with the P_{exp}'s given in table 2.

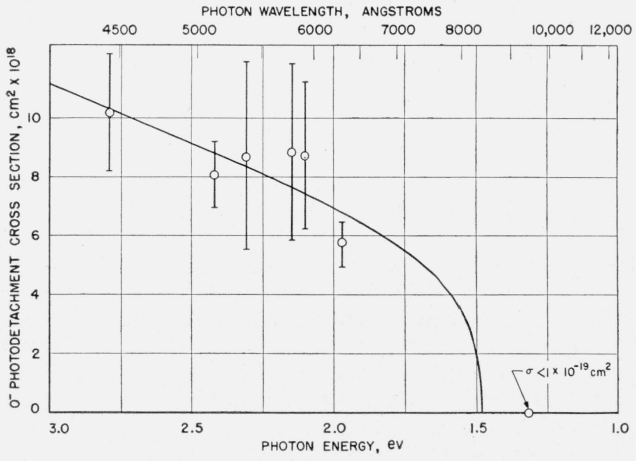

FIGURE 9. *The trial photodetachment cross section $\sigma'(\lambda)$, which is consistent with experimental results.*

Integrations of eq (1) using this cross section and the filter transmissions of figure 3 yield results which are given as P_{theo} in tables 2 and 6. Near threshold this trial cross section has the form given by eq (6) for nonresonant photodetachment.

The data given by the circles are obtained from eq (5); and are not used to determine the curve.

Where applicable, eq (5) has been used to obtain σ's associated with various ΔP_{exp}'s. This equation is used when the filters have the proper sharp cutoff and constant transmission short of cutoff, and where the P_{exp}'s seem to justify the assumption of a slowly varying cross section. The results are given in table 4 and plotted in figure 9 at the peak wavelengths associated with the differences of the filter transmissions. Note that the σ's obtained from eq (5) are not independent. An error in one P_{exp}

TABLE 1. *Comparison of the observed spectral distribution [a] of the photodetachment cross section for H^- with the theory of Chandrasekhar, relative to the results for filter 3486*

	Run A		Run B		
Corning filter No.	Number of measurements	Average relative P_{exp}/P_{theo}	Number of measurements	Average relative P_{exp}/P_{theo}	Mean deviation
3389	3	0.96	11	1.04	±0.04
3385	3	1.02	10	1.01	±.06
3486	5	(1.00)	11	(1.00)	±.03
3482	4	0.97	11	1.00	±.04
2424	3	.98	11	0.97	±.02
2412	3	1.02	10	.97	±.06
2030	2	1.00			
2550	2	0.99			
2540	4	.97			

[a] The absolute measurement of the integrated cross section for H^-, using filter 3486, is given in (2). The experimental results agree with the prediction of the theory within 2 percent and are estimated to be reliable within 10 percent.

TABLE 2. *Experimental photodetachment probability, P_{exp}, for O^- from an O_2 discharge with 10 glass filters and one interference filter; and P_{theo}, using eq (1) and the $\sigma'(\lambda)$ given in figure 9 and table 3 for a 1.48-ev affinity*

Corning filter No.	P_{exp} [a]	P_{theo}	$(P_{exp}-P_{theo})$
7380	$1.66\pm0.02\times10^{-5}$	1.69×10^{-5}	-0.03×10^{-5}
3385	1.50±0.04	1.48	+.02
3486	1.35±0.03	1.36	−.01
3482	1.25±0.04	1.24	+.01
2424	1.08±0.05	1.10	−.02
2412	0.95±0.07	0.984	−.03
2030	.82±0.03	.784	+.04
2600	.38±0.04	.363	+.02
2550	.074±0.016	.089	−.015
2540	<.02	.012	<.02
Reflection filter [b]	----------	.14	----------

[a] The errors are average deviations from the mean values of the experimental data from 21 experiments.

[b] The interference filter was used with O^- from a CO discharge. See table 6 for data from CO.

TABLE 4. *Values of the O^- photodetachment cross section [a] obtained from equation (5)*

Filter combination	λ_{peak}	Denominator eq (5)	Numerator eq (5)	σ
7380-3385	4400	0.865×10^{-11}	0.118 ±0.020 [b]	$0.102\pm0.017\times10^{-16}$
3385-3486	5120	.664	.121 ±0.014	.080 ±.009
3486-3482	5370	1.019	.086 ±0.029	.088 ±0.030
3482-2424	5770	0.540	.162 ±0.054	.087 ±0.029
3482-2412	5900	.353	.247 ±0.068	.087 ±0.024
2424-2030	6300	.268	.216 ±0.026	.058 ±0.007

[a] The values given in the fourth column are the averages of 21 independent differences of individual measurements for the indicated filter pairs.

[b] The errors are the average deviations from the mean.

TABLE 3. *Data* [a] *to be used in the integration of equation (1) for comparison of arbitrary cross sections σ (λ) with our experimental results*

$\lambda\mu$	$\mathcal{E}_{ev}$	T_{3385}	T_{3486}	T_{3482}	T_{2412}	T_{2424}	T_{2030}	T_{2600}	T_{2550}	T_{2540}	T_r	$\phi'_\lambda\lambda$	σ'
0.400	3.100	------	------	------	------	------	------	------	------	------	------	0.0588	[b] 11.77×10^{-18}
.408	3.039	------	------	------	------	------	------	------	------	------	------	------	------
.416	2.981	------	------	------	------	------	------	------	------	------	------	.0753	11.24
.424	2.925	------	------	------	------	------	------	------	------	------	------	------	------
.432	2.870	------	------	------	------	------	------	------	------	------	------	.0951	10.79
.440	2.818	------	------	------	------	------	------	------	------	------	------	------	------
.448	2.768	------	------	------	------	------	------	------	------	------	------	.1186	10.35
.456	2.719	------	------	------	------	------	------	------	------	------	------	------	------
.464	2.672	0.000	------	------	------	------	------	------	------	------	------	.1425	9.96
.472	2.627	.075	------	------	------	------	------	------	------	------	------	------	------
.480	2.583	.375	------	------	------	------	------	------	------	------	------	.1679	9.58
.488	2.541	.665	------	------	------	------	------	------	------	------	------	------	------
.496	2.500	.790	------	------	------	------	------	------	------	------	------	.1974	9.24
.504	2.460	.850	------	------	------	------	------	------	------	------	------	------	------
.512	2.422	.875	0.015	------	------	------	------	------	------	------	------	.2261	8.92
.520	2.385	.890	.240	------	------	------	------	------	------	------	------	------	------
.528	2.348	.900	.640	------	------	------	------	------	------	------	------	.2610	8.62
.536	2.313	.904	.790	0.000	------	------	------	------	------	------	------	------	------
.544	2.279	.906	.817	.125	------	------	------	------	------	------	------	.2902	8.33
.552	2.246	.908	.835	.475	------	------	------	------	------	------	------	------	------
.560	2.214	.909	.850	.725	------	------	------	------	------	------	------	.3235	8.04
.568	2.183	.910	.858	.810	------	------	------	------	------	------	------	------	------
.576	2.153	.910	.867	.835	------	0.007	------	------	------	------	------	.3574	7.77
.584	2.123	.910	.871	.847	------	.100	------	------	------	------	------	------	------
.592	2.095	.909	.880	.855	0.000	.375	------	------	------	------	------	.3898	7.50
.600	2.067	.908	.883	.862	.015	.675	------	------	------	------	------	------	------
.608	2.039	.907	.885	.866	.185	.800	------	------	------	------	------	.4251	7.24
.616	2.013	.906	.891	.870	.550	.850	------	------	------	------	------	------	------
.624	1.987	.905	.892	.875	.785	.865	------	------	------	------	------	.4583	7.02
.632	1.962	.904	.893	.876	.845	.875	------	------	------	------	------	------	------
.640	1.938	.903	.894	.880	.865	.883	0.000	------	------	------	------	.4897	6.72
.648	1.913	.902	.895	.882	.875	.888	.065	------	0.000	------	------	------	------
.656	1.890	.901	.896	.885	.880	.893	.425	------	.002	------	------	.5211	6.44
.664	1.867	.900	.897	.885	.883	.895	.650	------	.005	------	------	------	6.32
.672	1.845	.899	.898	.886	.885	.900	.775	------	.006	------	------	.5499	6.19
.680	1.823	.898	.898	.887	.886	.900	.850	------	.007	------	------	------	6.05
.688	1.802	.896	.899	.888	.888	.901	.870	------	.010	------	------	.5769	5.91
.696	1.781	.895	.899	.889	.889	.902	.877	------	.014	------	------	------	5.77
.704	1.761	.894	.898	.890	.889	.905	.883	------	.016	------	0.000	.6023	5.62
.712	1.742	.893	.897	.890	.888	.905	.885	0.015	.020	------	.002	.6145	5.48
.720	1.722	.892	.896	.889	.887	.905	.886	.125	.030	------	.004	.6267	5.30
.728	1.703	.891	.896	.888	.885	.905	.887	.300	.038	------	.005	.6406	5.20
.736	1.685	.890	.895	.886	.884	.905	.889	.500	.048	------	.008	.6498	5.10
.744	1.667	.889	.895	.883	.883	.905	.889	.635	.060	------	.011	.6600	4.97
.752	1.649	.883	.894	.882	.879	.905	.890	.710	.067	------	.020	.6716	4.83
.760	1.632	.882	.892	.881	.878	.905	.890	.760	.082	------	.034	.6823	4.68
.768	1.615	.881	.892	.880	.877	.905	.890	.785	.097	------	.055	.6917	4.50
.776	1.598	.880	.891	.880	.876	.905	.889	.795	.122	------	.100	.7022	4.30
.784	1.582	.879	.889	.878	.876	.905	.887	.800	.140	------	.200	.7106	4.08
.792	1.566	.878	.888	.877	.874	.905	.886	.799	.165	------	.350	.7188	3.82
.800	1.550	.877	.888	.876	.872	.905	.886	.795	.190	------	.600	.7276	3.52
.808	1.534	.876	.886	.875	.871	.905	.884	.790	.217	0.000	.815	.7342	3.18
.816	1.519	.874	.882	.873	.869	.905	.880	.780	.245	.005	.825	.7418	2.74
.824	1.505	.873	.881	.871	.868	.905	.879	.772	.275	.010	.725	.7494	2.23
.832	1.490	.873	.880	.870	.866	.905	.878	.764	.305	.015	.600	.7560	1.44
.840	1.476	.872	.879	.870	.864	.905	.877	.753	.337	.025	.520	.7617	0.00
.848	1.462	.871	.878	.868	.862	.905	.876	.742	.370	.035	.470	.7680	------
.856	1.449	.869	.877	.865	.861	.905	.875	.730	.401	.050	.450	.7740	------
.864	1.435	.868	.876	.864	.860	.905	.874	.718	.430	.063	------	.7796	------
.872	1.422	.867	.875	.864	.859	.905	.873	.705	.460	.080	------	.7858	------
.880	1.410	.867	.874	.862	.858	.905	.872	.690	.495	.100	------	.7916	------
.888	1.396	.867	.873	.861	.857	.905	.871	.675	.525	.125	------	.7945	------
.896	1.384	.867	.871	.860	.855	.905	.869	.657	.552	.150	------	.7985	------
.904	1.372	.867	.868	.859	.854	.905	.866	.642	.580	.175	------	.8022	------
.912	1.360	.866	.867	.857	.854	.905	.865	.625	.605	.215	------	.8062	------
.920	1.348	.865	.866	.856	.853	.905	.864	.605	.630	.250	------	.8105	------
.928	1.336	.863	.865	.855	.851	.905	.863	.584	.652	.280	------	.8112	------
.936	1.325	.863	.864	.854	.850	.905	.862	.563	.675	.310	------	.8136	------
.944	1.313	.863	.863	.854	.849	.905	.861	.539	.694	.345	------	.8159	------
.952	1.302	.863	.862	.853	.848	.905	.860	.516	.713	.375	------	.8192	------
.960	1.292	.863	.861	.852	.846	.905	.859	.488	.730	.405	------	.8217	------
.968	1.281	.863	.860	.850	.845	.905	.858	.457	.741	.437	------	.8223	------
.976	1.270	.863	.859	.850	.844	.905	.857	.425	.755	.465	------	.8242	------
.984	1.260	.862	.858	.850	.844	.905	.856	.390	.775	.495	------	.8243	------
.992	1.250	.862	.858	.850	.844	.905	.856	.355	.785	.520	------	.8261	------

[a] Heading symbols are defined in the text of this paper. See eq (1). T_r is the transmission of the interference reflection filter.
[b] Data for integration of the trial cross section shown in figure 9.

may be reflected in the error associated with more than one ΔP_{exp}. An attempt was made, by successive approximations, to obtain the smooth monotonic cross section that most nearly fits the data of table 2. This curve is plotted in figure 9. The σ's from this curve that were used in the numerical integration of eq (1) are given in table 3, and the results of the integration are given as P_{theo} in table 2.

The cross section for radiative attachment, of interest in upper atmosphere physics, was derived [18] from this curve using the principle of detailed balancing, and is given in figure 10 and table 5.

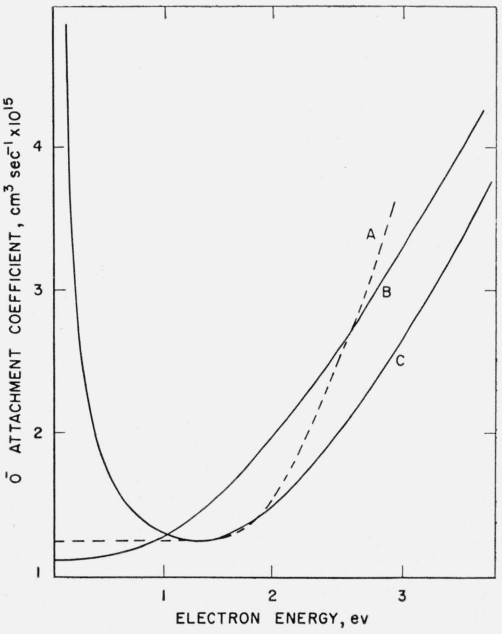

FIGURE 10. *Experimental and theoretical radiative attachment coefficients for atomic oxygen.*

The attachment coefficient is equal to the product of electron velocity and attachment cross section. Curve A is calculated from our trial cross section (see fig. 9) by the principle of detailed balancing. Curves B and C are calculated by Bates and Mass..y [4], B assuming no excited state near the continuum and C. assuming resonant capture of s electrons.

TABLE 5. *The radiative attachment coefficient α for atomic oxygen, calculated from the photodetachment "trial" cross section given in table 3*

Energy of the incident electron	α	Energy of the incident electron	α
ev	*cm³-sec⁻¹*	*ev*	*cm³-sec⁻¹*
1.62	3.44×10^{-15}	0.46	1.44×10^{-15}
1.50	3.15	.41	1.40
1.39	2.92	.37	1.35
1.29	2.70	.32	1.31
1.19	2.52	.28	1.27
1.10	2.35	.24	1.24
1.02	2.21	.21	1.24
0.94	2.09	.17	1.24
.87	1.98	.14	1.24
.80	1.87	.10	1.24
.73	1.78	.07	1.24
.67	1.70	.04	1.24
.62	1.62		
.56	1.55		
.51	1.50		

4.3. O^- Affinity

a. O^- from an O_2 Discharge

The threshold of the monotonic trial cross section that fits the experimental data for O^- from an O_2 discharge is about 1.48 ev. Upper and lower limits are immediately apparent if the P_{exp}'s (table 2) are compared with the filter transmission curves (fig. 3). The large detachment signal with filter 2600 shows that the threshold lies substantially below 1.75 ev. Because no signal is observed with filter 2540 [$\sigma(\lambda)<1\times10^{-19}$] cm^2], the threshold must be above 1.35 ev.

The shape of the cross section near the threshold is not uniquely determined by these experimental data. The threshold can be moved to slightly higher values on the electron-volt scale and remain in agreement with the experimental data through eq (1). This is allowable only if there is a sharp peak very near threshold, followed by a deep minimum, in order to account for the observed detachment with filter 2600.

b. O^- from a CO Discharge

After the completion of the experiments on O^- from oxygen discharges, the affinity and shape of the cross section near threshold were confirmed using ions from a discharge through carbon monoxide. The results prove that all the O_2^- ions had been eliminated from the O^- beam in the oxygen experiments. The concentration of O_2^- ions in the beam from the CO discharge was $\sim$0.1 percent of the beam current, compared to $\sim$50 percent from an O_2 discharge. Figure 11 shows the spectrum of the beam from CO, with the velocity selector turned off. The velocity selector removes the impurity peaks except for a negligible trace of C^-.

Table 6 shows the relative values of P_{exp} for a selected group of filters near the threshold, together with the corresponding P_{theo} ratios. Included with these data is a measurement with a multilayer interference reflection filter, the transmission characteristic of which is shown in figure 3. The de-

TABLE 6. *Experimental results of measurements made using O^- ions from a carbon monoxide discharge*

Filters	$\frac{P_{a_{theo}}{}^{a}}{P_{b_{theo}}}$	$\frac{P_{a_{exp}}}{P_{b_{exp}}}$
$\frac{\#1(\text{reflection})^{b}}{2424}$	0.127	0.17 ± 0.04^{c}
$\frac{2030}{2424}$	.713	$.715\pm.03$
$\frac{2600}{2030}$	.463	$.47\pm.03$
$\frac{2550}{2030}$	.114	$.16\pm.05$

[a] P_{theo}'s are calculated from the trial cross section given in table 3 and shown in figure 9.
[b] The filter transmission characteristics are shown in figure 3.
[c] The errors are the estimated reliabilities of the 2 or 3 measurements made with each filter.

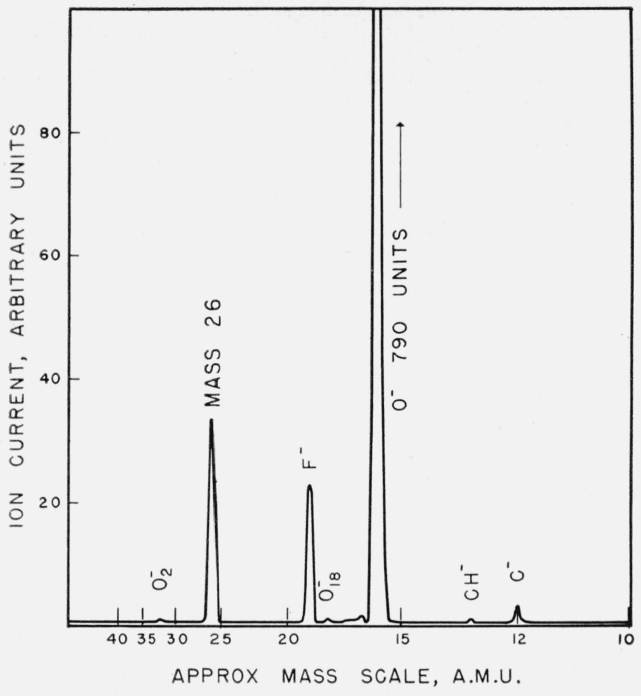

FIGURE 11. *Mass spectrum of the ion beam from a* CO *discharge.*

This spectrograph was taken with the 90° sector-field instrument. Mass 26 is not identified.

tachment signal obtained when this filter is placed behind the water cell, one face of which is filter 2424, proves that the oxygen affinity lies below 1.58 ev regardless of the shape of the curve. Within experimental error, the position of the threshold given by the ions from CO is the same as that given by the ions from O_2.

c. Discussion

The experimental results prove that the threshold lies between 1.55 and 1.35 ev. The identification of this threshold with the affinity would be taken for granted if the affinity were not in unresolved conflict with the generally accepted value of 2.2 ev [17]. The interpretation of our observed threshold as the threshold for detachment from a metastable excited state of O^- might resolve the conflict if this interpretation were not untenable. This state would necessarily lie about 0.5 ev above the ground state in order to be consistent with the 2.2 ev value of the affinity.

Bates and Massey [4], in an attempt to justify theoretically a $(2p)^4 3s$ excited configuration barely stable with respect to a 2.2-ev affinity, found that the polarization of the core of the ion "required to give a stable level was far in excess of the probable value" [19]. Bates [20] has calculated, by an empirical method, that a $(2p)^4 3s$ configuration should lie about 2 ev higher than the $(2p)^5$ configuration taken as the configuration of the ground state. Some experimental evidence has been presented in favor of a 2.2-ev affinity with an excited state lying very near to the continuum, but there is no evidence for an excited state appreciably below the continuum. The possibility that we are observing absorption from metastable ions is further reduced by the results with CO, for one would not expect CO and O_2 discharges to result in beams with equal concentrations of metastables. Use of our value of the affinity of oxygen may permit a reinterpretation of the electron impact data [21] without recourse to the assumption that negative ions are created in excited states.

For photodetachment from a $(2p)^5$ O^- ground-state configuration, in the absence of stable excited states, the shape of the cross section is restricted by the requirement [22] that near the threshold

$$\sigma(\lambda) \sim \lambda^2 (E_0 - hc/\lambda)^{1/2}. \tag{6}$$

This requires a zero slope for the attachment coefficient (fig. 10) and an infinite slope for the cross section at the threshold. This shape was used near the threshold of the trial cross section (see fig. 9).

The measured threshold for photodetachment from the ground state of O^-, the affinity, is 1.48 ± 0.10 ev. The assigned error is derived from (a) the theoretical requirement that the cross section must intersect the wavelength abcissa with infinite slope and (b) the certainty from the observation of a finite signal with the interference filter that the threshold lies at or below 1.55 ev. Shape of the cross section must be roughly that given by σ' in figure 9, but the possibility of irregularities or fine structure is not excluded. It is quite unlikely that there exists a resonant peak at the threshold.

We are grateful to many members of the NBS staff for help in the calibration of various parts of the apparatus, particularly John Schleter, Nicholas Acquista, Russel Johnston, and Marion Belknap. Victor Grob carried out the many tedious numerical integrations and assisted with the operation of the equipment. Most of the construction of the apparatus was accomplished by Adolph Huriaux. We are indebted to the evaporation group of Baird Associates, Inc., for the development of the special interference filter. Suggestions by A. Dalgarno, D. R. Bates, Wade Fite, and Homer Hagstrum have been very helpful.

5. References

[1] L. M. Branscomb and W. L. Fite, Phys. Rev. [A] **93,** 651 (1954).
[2] L. M. Branscomb and S. J. Smith, Experimental cross section for photodetachment of electrons from H— and D—, Phys. Rev. **98,** 1028 (1955).
[3] S. Chandrasekhar, Astrophys. J. **102,** 395 (1945).
[4] D. R. Bates and H. S. W. Massey, Trans. Roy. Soc. (London) [A] **239,** 269 (1943).
[5] H. S. W. Massey, Negative ions, p. 21 (University Press, Cambridge, England, 1950).
[6] H. S. W. Massey, Negative ions, p. 36 (University Press, Cambridge, England, 1950).
[7] L. M. Branscomb and S. J. Smith, The electron affinity of atomic oxygen, Phys. Rev. (L) **98,** 1127 (1955).
[8] Massey, loc. cit., p. 3 ff.

[9] H. D. Hagstrum, Phys. Rev. **23,** 185 (1951).
[10] J. B. Hasted, Proc. Roy. Soc. (London) [A] **212,** 235 (1952).
[11] J. B. Hasted, Proc. Roy. Soc. (London) [A] **222,** 74 (1954).
[12] Handbook of Chemistry and Physics, 35th ed., p. 2466 (Rubber Publishing Co., Cleveland, 1953).
[13] D. B. Judd, J. Research NBS **44,** 1 (1950) RP2053.
[14] J. C. DeVos, The emissivity of tungsten ribbon (Dissertation, Univ. of Amsterdam 1953).
[15] K. S. Gibson, Phys. Rev. **7,** 194 (1916).
[16] W. L. Fite, Phys. Rev. **89,** 411 (1953).
[17] H. O. Pritchard, Chem. Rev. **52,** 529 (1953).
[18] L. M. Branscomb and S. J. Smith, Trans. A. G. U. to be submitted.
[19] H. S. W. Massey, Negative ions, p. 21 (University Press, Cambridge, England, 1950).
[20] D. R. Bates, Proc. Roy. Irish Acad. [A] **51,** 151 (1947).
[21] H. D. Hangstrum (private communication, 1955).
[22] H. S. W. Massey, Negative ions, p. 33 (University Press, Cambridge, England, 1950).

WASHINGTON, April 7, 1955.